Septin GTPases spatially guide microtubule organization and plus end dynamics in polarizing epithelia

Jonathan R. Bowen, Daniel Hwang, Xiaobo Bai, Dheeraj Roy, and Elias T. Spiliotis

Department of Biology, Drexel University, Philadelphia, PA 19104

Establishment of epithelial polarity requires the reorganization of the microtubule (MT) cytoskeleton from a radial array into a network positioned along the apicobasal axis of the cell. Little is known about the mechanisms that spatially guide the remodeling of MTs during epithelial polarization. Septins are filamentous guanine triphosphatases (GTPases) that associate with MTs, but the function of septins in MT organization and dynamics is poorly understood. In this paper, we show that in polarizing epithelia, septins guide the directionality of MT plus end movement by suppressing MT catastrophe. By enabling persistent MT growth, two spatially distinct populations of septins, perinuclear and peripheral filaments, steer the growth and capture of MT plus ends. This navigation mechanism is essential for the maintenance of perinuclear MT bundles and for the orientation of peripheral MTs as well as for the apicobasal positioning of MTs. Our results suggest that septins provide the directional guidance cues necessary for polarizing the epithelial MT network.

Introduction

The morphogenesis and physiology of polarized epithelia are intimately linked to the organization of the microtubule (MT) cytoskeleton (Müsch, 2004). During polarization, epithelial MTs are reorganized from a radial array into a network, which consists of MT bundles that align along the lateral membrane, and a meshwork of MTs that are positioned under the apical and basal membrane (Bacallao et al., 1989). This network underlies the sorting and polarized trafficking of membrane proteins that maintain homeostasis across the epithelial barrier (Mostov et al., 2003; Rodriguez-Boulan et al., 2005; Mellman and Nelson, 2008). In contrast to membrane traffic, which has been studied extensively, little is known about the mechanisms that control the spatial organization of the epithelial MT network.

Remodeling of epithelial MTs is initiated by cell adhesion cues and changes in Par1 signaling (Rodriguez-Boulan and Nelson, 1989; Chausovsky et al., 2000; Waterman-Storer et al., 2000; Cox et al., 2001; Doerflinger et al., 2003; Cohen et al., 2004). Subsequently, the MT-organizing center is dispersed (Buendia et al., 1990), and MTs reorganize by active movement, bundling, and anchoring to the plasma membrane (Bacallao et al., 1989; Bré et al., 1990; Pepperkok et al., 1990). Membrane anchoring involves the tumor suppressor adenomatous polyposis coli and the pleckstrin homology–like domain family A protein LL5, which associate with the basal membrane and interact with MT plus end–tracking proteins (+TIPs; Su et al., 1995; Mogensen et al., 2002; Reilein and Nelson, 2005; Hotta et al., 2010). Together with +TIPs and the kinesin KIF17, adenomatus polyposis coli also affects MT stability, which increases as epithelial cells polarize (Bré et al., 1987, 1990; Zumbrunn et al., 2001; Jaulin and Kreitzer, 2010). Despite this knowledge, the mechanisms that spatially guide MT movement and bundling are unknown.

Septins are heteromeric filamentous GTPases with evolutionarily conserved roles in cell polarity (Caudron and Barral, 2009; McMurray and Thorner, 2009). In budding yeast, septins associate with the cell cortex and are essential for polarized membrane growth and cell division (McMurray and Thorner, 2009; Oh and Bi, 2011). During yeast mitosis, cortical attachment and shrinkage of MTs involve septins and Par1-like, septin-dependent kinases (Kusch et al., 2002). In mammalian epithelia, septins associate with a subset of MTs and facilitate vesicle transport during polarization (Spiliotis et al., 2008).

Correspondence to Elias T. Spiliotis: ets33@drexel.edu

Abbreviations used in this paper: CLASP, CLIP-associated protein; CTT, C-terminal tail; fps, frame per second; MT, microtubule; shRNA, small hairpin RNA; +TIP, plus end–tracking protein.

The Rockefeller University Press $30.00
J. Cell Biol. Vol. 194 No. 2 187–197
www.jcb.org/cgi/doi/10.1083/jcb.201102076

Septins have been indirectly implicated in the posttranslational modifications and stability of MTs (Nagata et al., 2003; Kremer et al., 2005; Spiliotis et al., 2008), but the functional significance of the MT association with septins is not understood.

Here, we show that septins guide the growth of epithelial MTs by suppressing MT catastrophe in perinuclear and peripheral regions of the cytoplasm. Thereby, MT-associated septins direct the longitudinal bundling of perinuclear MTs and the membrane targeting of peripheral MTs. Surprisingly, septins provide a navigation mechanism for the growth and positioning of MTs along the axis of apicobasal polarity.

Results and discussion

To examine the role of septins in the spatial organization of MTs during epithelial polarization, we focused our experiments on the ubiquitous SEPT2–6–7 complex, which has been shown to form filaments in MDCK cells (Joberty et al., 2001), an in vitro model of epithelial polarity. Because MT reorganization begins with the formation of MDCK cell–cell adhesions (Bacallao et al., 1989; Chausovsky et al., 2000; Waterman-Storer et al., 2000), we localized septins in cells, which had developed cell–cell contacts but were not confluent enough to become fully polarized. In these polarizing cells, the MT network lacked radial morphology and consisted of MTs with diverse orientation and morphology (Fig. 1 A).

Septin filaments demarcate two spatially distinct populations of MTs

Using antibodies against SEPT2, we identified two populations of septin filaments: perinuclear filaments, which were long and thick (Fig. 1 A), and peripheral filaments of shorter and stubbier appearance, which localized in close proximity to paxillin-enriched focal adhesions at the free lamellar edges of the cell (Fig. 1 B). These filamentous populations also contained SEPT6 and SEPT7 (Fig. S1 A). Peripheral SEPT2-containing filaments partially overlapped with the distal ends of MTs (Fig. 1 B, insets), and perinuclear SEPT2 colocalized extensively with longitudinal MTs (Fig. 1 A, insets), which run parallel or at shallow angles (5–20°) to the long axis of the cell (Fig. 1 C). In serial confocal microscopy sections, longitudinal MTs stained brighter for α-tubulin, indicating that these might be bundles of overlapping MTs. Based on a previous study that used fluorescence microscopy to distinguish between single and bundled MTs (Sammak and Borisy, 1988), we developed an automated script to mask perinuclear MTs with fivefold or more the intensity of the dimmest peripheral MTs and quantified colocalization with SEPT2. Strikingly, SEPT2 showed preferential colocalization with putative MT bundles compared with total MTs (Fig. 1 D).

To test whether SEPT2 preferentially associates with MT bundles, we treated MDCK cells with paclitaxel, an MT-stabilizing drug that enhances lateral MT contacts and, thereby, induces the formation of MT bundles (Downing, 2000). Concomitant to MT bundling, paclitaxel induced the proliferation of SEPT2 filaments (Fig. S1 B). Because MTs buckle under the force of cargo-bound motors (Kulic et al., 2008), we reasoned that MT bundles should be more resilient to bending than unbundled MTs. Time-lapse imaging of α-tubulin–GFP and SEPT2-mCherry showed that SEPT2-associated MTs were significantly less prone to buckling and side to side movements than SEPT2-free MTs (Fig. 1, E and F). Collectively, these data demonstrate that in polarizing epithelia, septins demarcate two spatially and qualitatively distinct populations of MTs.

Septins are essential for the organization of perinuclear and peripheral MTs

To test whether septins affect the organization of epithelial MTs, we perturbed the native function of SEPT2 by knocking down its expression and, alternatively, by introducing a dominant-negative SEPT2 construct. First, subconfluent MDCKs were transfected with pSUPER-GFP plasmids expressing small hairpin RNAs (shRNAs) that targeted the canine SEPT2. As reported previously (Kinoshita et al., 2002), SEPT2 knockdown also reduced the expression and filamentous appearance of SEPT6 and SEPT7 (Fig. S1 C). In contrast to controls, septin-depleted cells lacked longitudinal MTs (Fig. 2 A). To assess whether septin depletion decreases the number of MT bundles, we quantified MT bundles as the percentage of total MTs. SEPT2 knockdown led to a >50% reduction in MT bundles; this result was reproducible with three different shRNAs against SEPT2 (Fig. 2, A and B). Consistent with a reduction in MT bundles, we observed an increase in MT buckling and side to side movements (Fig. S2, A and B).

Because shRNAs can have nonspecific and off-target effects, we sought to reproduce our data with a dominant-negative SEPT2 construct. We constructed a GFP-tagged chimera of SEPT2 that lacked its C-terminal tail (CTT), which contains coiled-coil protein-binding domains and is critical for the lateral pairing of septin oligomers (Bertin et al., 2008). To assess whether SEPT2-ΔCTT behaved as a dominant negative, we analyzed its effects on cytokinesis, which is acutely affected by SEPT2 (Kinoshita et al., 1997; Joo et al., 2007). We found that in cytokinetic SEPT2-ΔCTT-GFP–expressing cells (n = 22), intercellular bridges were wider (1.9 ± 0.3 vs. 1.1 ± 0.4 µm; P = 0.0005) and longer (6.5 ± 0.5 vs. 3.8 ± 0.5 µm; P = 0.0005) than in SEPT2-GFP expressors (n = 18). This phenotype was accompanied by an increase in the percentage of cells in cytokinesis. In interphase cells, SEPT2-ΔCTT phenocopied the effects of SEPT2 depletion, reducing MT bundles by more than half (Fig. 2 B and Fig. S2 C). Thus, septins are essential for the maintenance of perinuclear MT bundles.

Next, we examined the organization of peripheral MTs. In control cells, the preponderance of peripheral MTs pointed perpendicular to the cell edge with their distal ends slightly bent (Fig. 1 B and Fig. 2, C and D). In SEPT2-depleted cells, peripheral MTs run parallel to the cell edge, and their distal ends were tilted at steeper angles from the cell radius (Fig. 2, C and D). This phenotype was reminiscent of defective MT anchoring to the cortical membrane (Kodama et al., 2003; Mimori-Kiyosue et al., 2005). We concluded that, in addition to their role in the maintenance of perinuclear MT bundles, septins also affect the cortical targeting of peripheral MTs (also see Fig. 4 G).

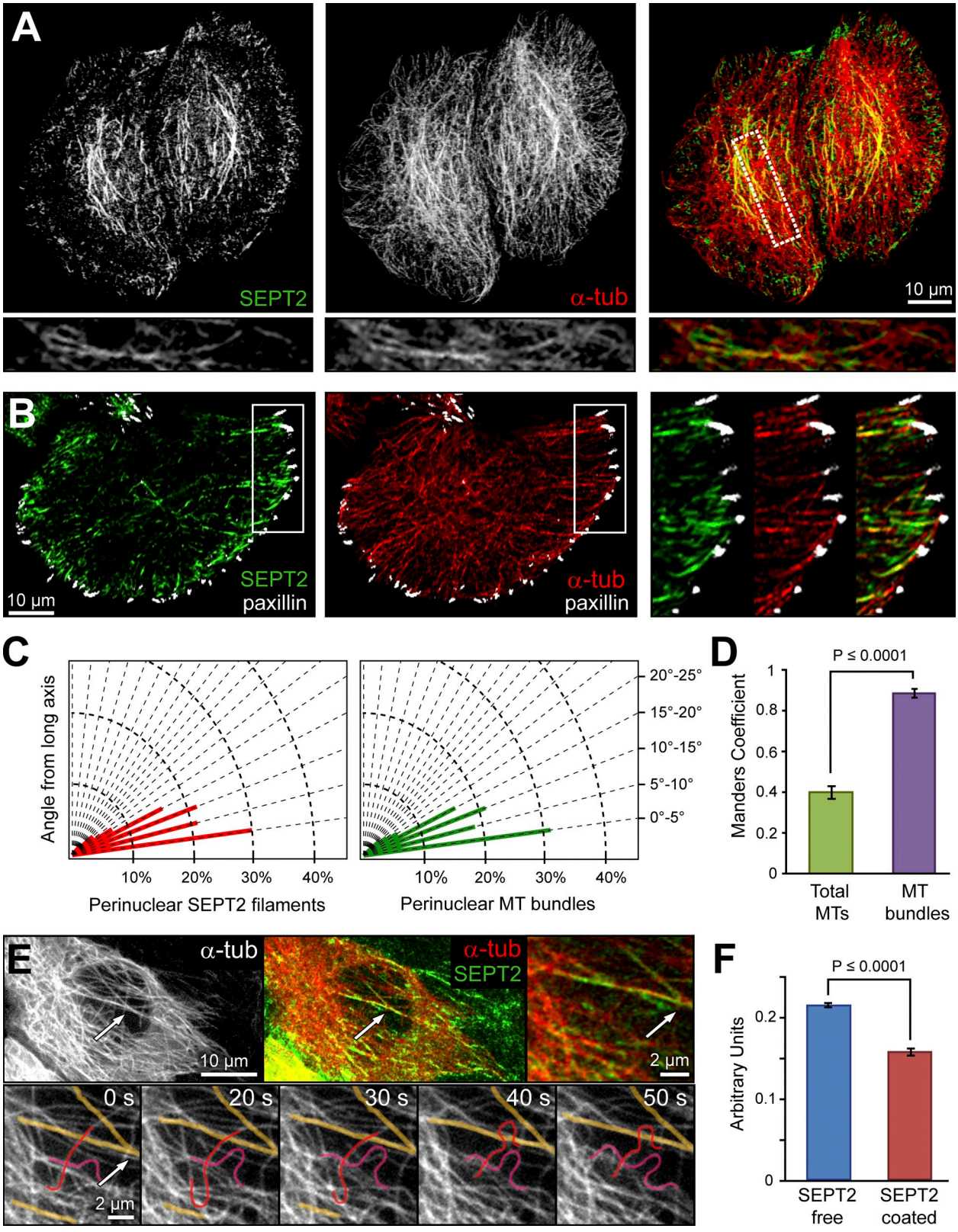

Figure 1. **Spatial segregation of septins within the MT network.** (A) Maximum intensity projection of confocal microscopy z stacks of MDCKs stained for SEPT2 and α-tubulin. (bottom) A single confocal slice from the outlined area in high magnification. (B) Confocal microscopy image of MDCKs stained for SEPT2, α-tubulin, and paxillin. (right) High magnification images of the outlined region. (C) Distribution of the angles of perinuclear SEPT2 filaments ($n = 177$) and MT bundles ($n = 155$) from the long axis of the cells ($n = 14$). (D) Manders coefficients of SEPT2 colocalization with total MTs and MT bundles ($n = 14$ cells). (E) Spinning-disk confocal microscopy images of MDCK-SEPT2-mCherry cells transfected with α-tubulin (α-tub)–GFP. Arrows point to SEPT2-coated MTs (pseudocolored yellow in grayscale images). MTs free of SEPT2 were pseudocolored red. (F) Quantification of MT fluctuations using image subtraction analysis ($\Delta t = 15$ s). Graph shows changes in α-tubulin–GFP intensity values per micrometers squared for SEPT2-mCherry–coated and –free MTs relative to total MTs (8 cells; $n = 50$). Error bars represent SEM.

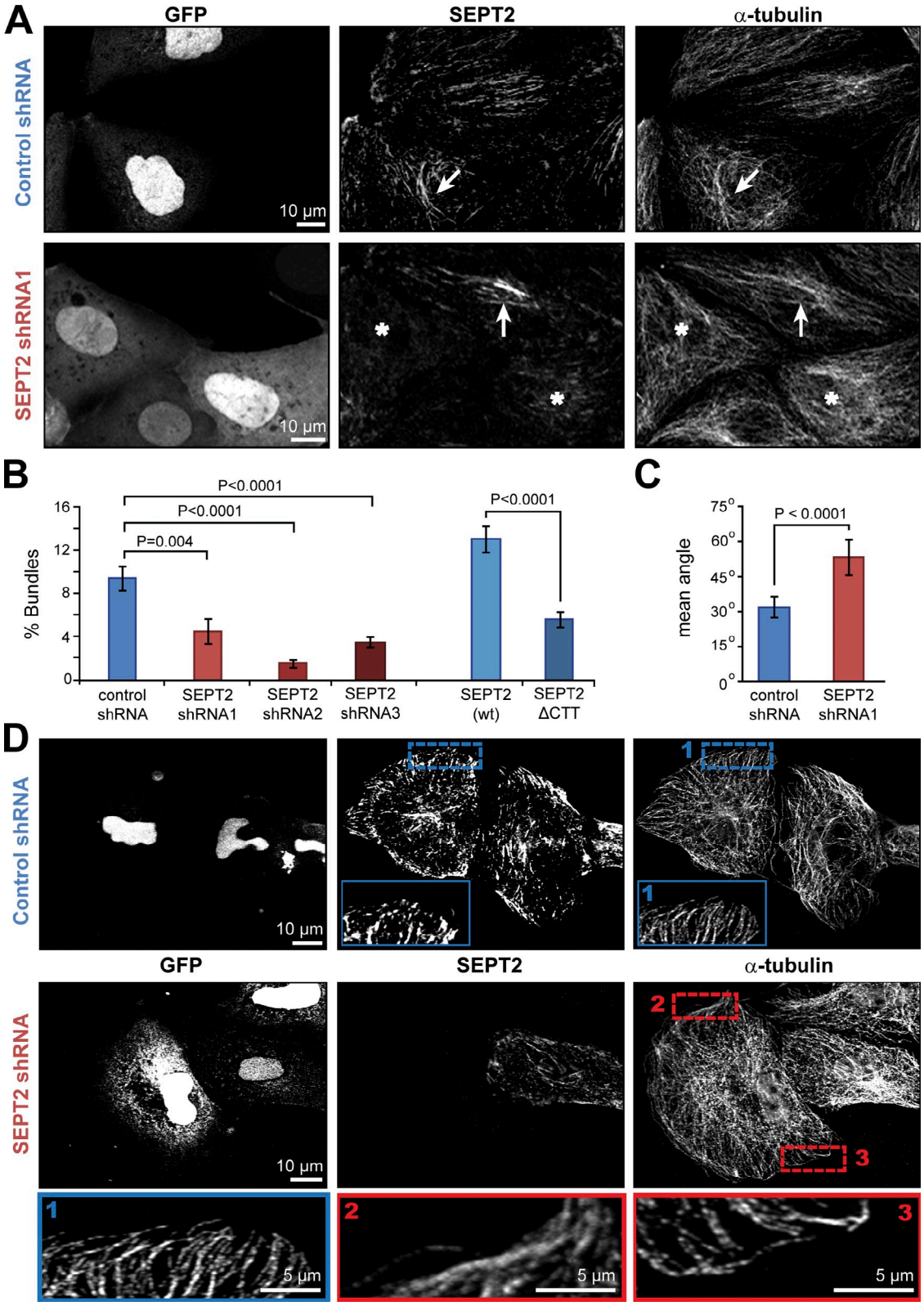

Figure 2. **Septins are essential for the organization of perinuclear MT bundles and peripheral MTs.** (A) Maximum intensity projections of confocal microscopy z stacks of MDCKs transfected with GFP-expressing control and SEPT2 shRNA 1 plasmids and stained for SEPT2 and α-tubulin. Arrows point to perinuclear longitudinal MT bundles. Asterisks mark SEPT2-depleted cells. (B) Quantification of MT bundles as the percentage of total MTs in cells transfected with control shRNA (n = 18), SEPT2 shRNA 1 (n = 15), shRNA 2 (n = 12), shRNA 3 (n = 13), GFP-tagged SEPT2 (n = 18), and SEPT2-ΔCTT (n = 21). (C) Graph shows the mean angle width between the distal ends of peripheral MTs and the effective cell radius (line between MT tips and the centroid of the cell) in MDCKs treated with control (10 cells; n = 50) and SEPT2 shRNAs (10 cells; n = 50). (D) Confocal microscopy images of MDCKs transfected with GFP-expressing control and SEPT2 shRNA and stained for α-tubulin. Insets show the distal ends of peripheral MTs in higher magnification. Error bars represent SEM. wt, wild type.

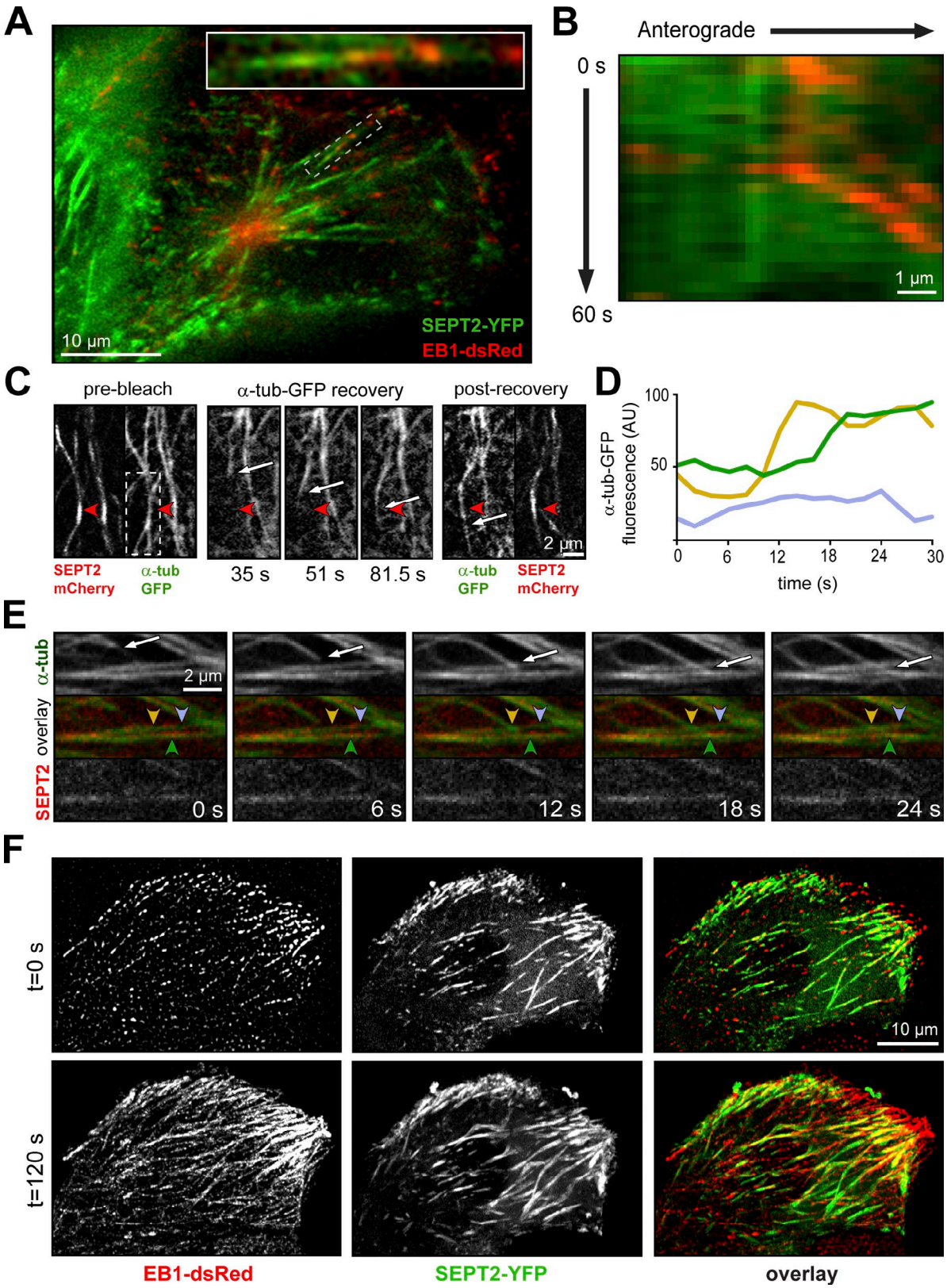

Figure 3. **MT plus ends follow trajectories that coalign with septin filaments.** (A) MDCK cells expressing EB1-dsRed and SEPT2-YFP. The inset shows EB1-dsRed comets that localize on a perinuclear SEPT2-YFP filament in high magnification. (B) Kymograph depicts the movement of EB1-dsRed along SEPT2-YFP. (C) FRAP of α-tubulin (α-tub)–GFP in MTs coated with SEPT2-mCherry. The dashed line demarcates the region of FRAP. Arrows point to MT tips. Arrowheads mark the position of SEPT2-mCherry. (D and E) Time-lapse images show docking and coalignment of an MT tip (arrows) with MTs coated with SEPT2-mCherry. Line graph shows the fluorescence intensity of α-tubulin–GFP at sites of MT–MT docking (yellow arrowheads) and alignment (green arrowheads) and at a point of no MT overlap (blue arrowheads). Note that α-tubulin–GFP intensity increases at points of MT overlap. (F) Spinning-disk confocal microscopy images of EB1-dsRed and SEPT2-YFP. Still frames and time-composite images are depicted in the top and bottom rows, respectively. AU, arbitrary unit.

Table I. **Quantification of MT plus end dynamics**

Parameter	Cell interior		Cell periphery	
	Control siRNA	SEPT2 siRNA	Control siRNA	SEPT2 siRNA
Growth rate (μm/min)	8.92 ± 0.4030	9.42 ± 0.6647	*5.32 ± 0.23*	*4.18 ± 0.17*[b]
Shortening rate (μm/min)	11.8 ± 1.7474	14.9 ± 1.8596	7.09 ± 0.44	6.65 ± 0.41
Catastrophe rate (μm/min)	19.4 ± 3.8667	18.1 ± 2.3859	10.1 ± 0.99	9.18 ± 0.74
Attenuation duration (s)	9.45 ± 0.9234	11.3 ± 1.0191	12.5 ± 0.83	11.1 ± 0.64
Transition frequency (s^{-1})				
Shortening to growth	0.018 ± 0.003	0.017 ± 0.003	0.024 ± 0.002	0.025 ± 0.002
Growth to shortening	0.019 ± 0.003	0.018 ± 0.003	0.025 ± 0.002	0.028 ± 0.003
Growth to catastrophe	*0.004 ± 0.002*	*0.013 ± 0.002*[a]	*0.006 ± 0.001*	*0.009 ± 0.001*[a]
Percent time				
Growth	84.1 ± 3.0123	80.4 ± 3.3093	*58.3 ± 2.74*	*49.4 ± 2.62*[a]
Shortening	8.87 ± 1.6971	11.9 ± 2.5739	*22.9 ± 2.11*	*30.1 ± 2.30*[a]
Catastrophe	*3.56 ± 1.1483*	*9.64 ± 2.5314*[a]	*9.85 ± 1.92*	*16.1 ± 2.29*[a]
Attenuation	35.1 ± 2.2910	34.9 ± 1.4142	18.8 ± 2.36	20.5 ± 2.41

MDCK-EB1-dsRed cells were simultaneously transfected with α-tubulin–GFP and control or SEPT2 siRNAs. EB1-dsRed displacements were quantified as described in Materials and methods. All values are means ± SEM. Values with statistically significant differences between control and SEPT2 siRNAs are highlighted in italics. Cell interior control siRNA: $n = 50$; 13 cells. Cell interior SEPT2 siRNA: $n = 50$; 16 cells. Cell periphery control siRNA: $n = 117$; nine cells. Cell periphery SEPT2 siRNA: $n = 104$; seven cells.

[a]$P < 0.05$.

[b]$P < 0.001$.

Tracking of MT plus ends along septins

In light of a recent study indicating that MT bundles are maintained by rescue of MT plus end shrinkage (Bratman and Chang, 2008), we reasoned that septins could affect the organization of both perinuclear MT bundles and peripheral MTs by modulating the dynamics of MT plus ends. To explore this hypothesis, we first set out to image the spatiotemporal dynamics of MT plus ends with respect to SEPT2.

Time-lapse imaging of the MT plus end protein EB1-dsRed and SEPT2-YFP showed that MT plus ends move anterogradely along septin filaments as they emerge from the perinuclear centrosomal region of the cell (Fig. 3, A and B; and Video 1). This was not an artifact of EB1-dsRed expression because endogenous EB1 also colocalized with perinuclear SEPT2 (Fig. S3 A). MT growth along perinuclear SEPT2 filaments was also observed using spinning-disk confocal microscopy combined with FRAP of α-tubulin–GFP (Fig. 3 C and Video 2). After photobleaching of MTs that were decorated with SEPT2-mCherry, MT ends (Fig. 3 C, arrows) extended along a path outlined by SEPT2-mCherry (Fig. 3 C, arrowheads). Anterograde movement of MT ends along perinuclear SEPT2 filaments indicated that SEPT2 is positioned along bundles of parallel MTs, which undergo persistent growth. Interestingly, these bundles were often targeted by individual MTs, which docked and then continued moving along SEPT2 (Fig. 3, D and E; and Video 3). Turning of MT plus ends onto septins was also apparent near the cell periphery (Fig. 3 F), where shorter septin filaments show little colocalization with MT lattices (Fig. 1, A and B). Peripheral MT plus ends followed trajectories that colocalized with peripheral SEPT2 filaments (Fig. 3 F and Video 4). Collectively, these data indicate that MT plus ends move on paths demarcated by septin filaments. Thus, septins may bias the directionality of MT growth by modulating the growth and shrinkage of MT plus ends.

Septins suppress MT plus end catastrophe and spatially guide MT growth and positioning

To test whether septins affect MT dynamic instability, we analyzed the parameters of EB1-dsRed dynamics in MDCKs transfected with α-tubulin–GFP and control or SEPT2 siRNAs. In the cell interior, SEPT2 RNAi affected only the frequency and duration of MT catastrophes (Table I). In SEPT2-depleted cells, MT catastrophes tripled, and MTs spent approximately three times as much time in catastrophe than control cells. At the cell periphery, SEPT2 knockdown increased the frequency and duration of MT catastrophes but also decreased the rate and duration of peripheral MT growth (Table I). In SEPT2-depleted cells, peripheral MTs spent 50% more time in the shortening phase than in control cells (Table I). These data indicate that septins protect both perinuclear and peripheral MTs from catastrophic depolymerization, maintaining MTs in a state of persistent growth.

Next, we examined whether septins affect the directionality of MT growth. Upon SEPT2 RNAi, MT plus end trajectories became highly entangled (Fig. 4 A). SEPT2 knockdown caused an increase in the number of EB1 trajectories that laterally intersected one another (Fig. 4, A and B). Overall, MT plus ends meandered through the cytoplasm rather than moving straight toward the periphery of the cell (Fig. 4 C). We reasoned that this phenotype could be caused by a failure in the docking and turning of MTs on septin-coated MT bundles (Fig. 3 E). In control cells, ∼30% of MT plus ends paused or turned while encountering an MT lattice (Fig. 4, D and E). This percentage did not change upon SEPT2 knockdown, but there was a significant decrease in the turning events (Fig. 4 E). This effect was not caused by a change in the angles of intermicrotubule collisions (Fig. 4 F), which in plants, are posited to influence MT–MT capture and alignment (Dixit and Cyr, 2004). Loss of

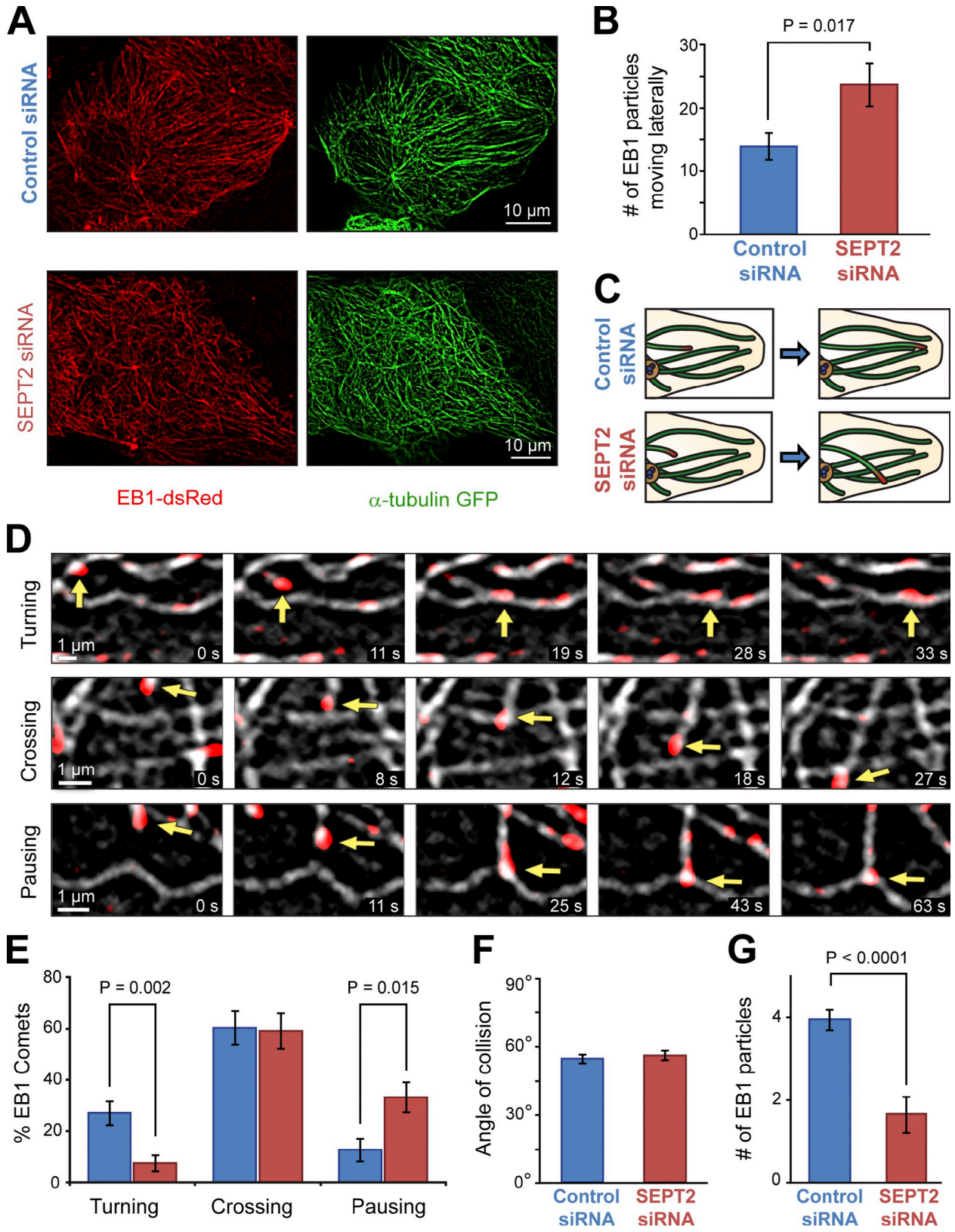

Figure 4. **Septins spatially guide MT growth and MT–MT interactions.** (A) Time-composite images of EB1-dsRed and α-tubulin–GFP after the lapse of 60 s. MDCK-EB1-dsRed cells were transfected with α-tubulin–GFP and control/SEPT2 siRNAs. (B) Graph shows the mean number of intersecting EB1-dsRed trajectories after a lapse of 60 s per control (n = 18) and SEPT2-depleted (n = 20) cells. (C) Schematic depicts the lateral meandering of MT plus ends in the absence of SEPT2. (D) Dual-color time-lapse images of α-tubulin–GFP (grayscale) overlaid with EB1-dsRed (red). Panels depict three types of MT–MT interactions. Yellow arrows point to MT plus ends moving through the cytoplasm. (E and F) Quantification of EB1-dsRed head-on encounters with MTs in MDCKs transfected with α-tubulin–GFP and control (10 cells; n = 99) and SEPT2 siRNAs (12 cells; n = 98). Right histogram shows mean angle width of all EB1-MT encounters. Data were analyzed from 90-s-long videos. (G) MDCK-EB1-dsRed cells were transfected with paxillin-GFP and control and SEPT2 siRNAs. Graph shows mean number of EB1-dsRed particles that enter a focal adhesion per 60 s (five cells; n = 20–25). Error bars represent SEM.

directionality in MT plus end movement was further confirmed by analyzing MT targeting to focal adhesions (Kaverina et al., 1998; Krylyshkina et al., 2003). SEPT2 knockdown resulted in a significant decrease in the number of EB1-dsRed comets that entered paxillin-GFP–enriched focal adhesions (Fig. 4 G). Therefore, septins not only are critical for persistent MT growth but also influence the directionality of MT plus end movement, which might be important for the positioning of the MT network during epithelial polarization.

Compared with contact-naive nonpolarized cells, in which SEPT2 is heavily distributed along the cell periphery (Fig. 5 A and Video 5), SEPT2 in polarizing MDCKs localizes to MT bundles that transverse the apex and sides of the nucleus (Fig. 5 B and Video 6). As epithelial cells become more columnar, septin filaments arch back along the lateral membrane (Fig. 5 C and Video 7) and in fully polarized cells, colocalize with vertically oriented lateral MT bundles (Fig. 5 D and Video 8). This spatial rearrangement correlates with the establishment of the apical MT meshwork, suggesting that septins could initially guide the movement of MTs toward the apical side of polarizing cells. Note that in confluent monolayers of MDCKs, EB1 comets appear docked at lateral septin filaments (Fig. S3, B and C). To test whether guidance of MT movement by SEPT2 is essential for the apicobasal positioning of epithelial MTs, subconfluent MDCKs were treated with control and SEPT2 siRNAs and then cultured at high density on Transwell filters to enable apicobasal expansion. We quantified the 3D distribution of MTs by determining the relative percentage of MT plus ends found in the apical, medial, and basal cytoplasm. Depletion of endogenous SEPT2 decreased the percentage of MT plus ends found in the apical cytoplasm, causing a shift in the distribution of MTs toward the basal and medial cytoplasm (Fig. 5, E and F). Collectively, these data indicate that septins navigate the growth and positioning of epithelial MTs during the establishment of apicobasal polarity.

Conclusions

More than 20 years ago, pioneering studies showed that epithelial polarization is accompanied by changes in the dynamic instability and spatial positioning of MTs (Bacallao et al., 1989; Bré et al., 1987, 1990; Pepperkok et al., 1990). To date, however, the molecules and mechanisms that guide the remodeling of epithelial MTs remain largely unknown. Here, we have uncovered a novel role for septins in coordinating MT plus end dynamics with MT organization. We have shown that guidance of MT plus ends takes place along a template of septin filaments, which maintain MTs in a state of directional and persistent growth, affecting the spatial organization of the epithelial MT network.

Previous work has shown that septins and Par-1–related kinases are required for the proper positioning of the mitotic spindle in budding yeast (Kusch et al., 2002). Although we cannot exclude a role for septins in epithelial Par1 signaling, SEPT2 is highly reminiscent of spectraplakins and CLIP-associated proteins (CLASPs), which affect MT organization in the cell body and periphery (Kodama et al., 2003; Mimori-Kiyosue et al., 2005; Wittmann and Waterman-Storer, 2005; Applewhite et al., 2010). Functionally, septins closely resemble the role of CLASPs in persistent MT growth, bundling, and capture (Akhmanova and Steinmetz, 2008; Bratman and Chang, 2008). Unlike CLASPs, however, septins do not appear to track on MT plus ends. We posit that septins interact transiently with +TIPs, including MT motors, which could mediate the turning of MT plus ends along septin-coated MTs. Interestingly, SEPT7 interacts with CENP-E (centromere-associated protein E), which was recently found in a complex with CLASPs (Zhu et al., 2008; Maffini et al., 2009), and whose kinesin 7 relatives Kip2/Tea2 track on MT plus ends (Browning et al., 2000; Carvalho et al., 2004; Zhu et al., 2008). Future studies will screen for septin interactions with +TIPs.

Overall, septins emerge as a unique class of filamentous microtubule-associated proteins that modulate MT dynamics and organization. Although a previous study had hinted at a role of septins in MT organization, the functional significance of the MT–septin interaction has only been the subject of speculation (Spiliotis, 2010). Our findings are consistent with the loss of MT polymer mass upon SEPT9 depletion (Nagata et al., 2003) and do not rule out the possibility that other septins (e.g., SEPT7) have additional or independent roles in the posttranslational modification and stability of MTs (Kremer et al., 2005). In MDCK epithelia, however, SEPT2 shows no significant colocalization with acetylated or detyrosinated MTs (Spiliotis et al., 2008). In light of recent evidence showing that septin overexpression strongly correlates with cancer resistance to MT-targeting drugs (Amir and Mabjeesh, 2007), our findings open a new path toward understanding how septin abnormalities contribute to the pathology of cancer.

Materials and methods

Tissue culture and transfections

MDCKII/G cells and the stable MDCK-EB1-dsRed (Barth et al., 2002), MDCK-SEPT2-YFP (Spiliotis et al., 2005), and MDCK-SEPT2-mCherry cell lines were maintained in low glucose DME with 1 g/liter $NaHCO_3$ and 10% FBS. Cells were seeded at 5×10^4 on 22-mm coverslips or 35-mm MatTek glass dishes or at 3×10^6 on Costar Transwell (6-well) filters coated with rat tail collagen. 1.5 µg plasmids and 0.1 µM siRNAs were transfected with Lipofectamine 2000 (Invitrogen). Before live-cell imaging, cells were switched into phenol red–free media supplemented with 20 mM Hepes (Invitrogen).

Plasmids and siRNAs

Control and SEPT2 shRNA constructs were made by subcloning SEPT2 shRNA 1, 5′-GGAGAACATCGTGCCCGTC-3′; shRNA 2, 5′-CCTTAGACGTCGCATTCATGAAA-3′; shRNA 3, 5′-TGAGTTCACACTAATGGTGGTCG-3′; and control shRNAs, 5′-GCCAGCGTGCGGTACAACT-3′ and 5′-GCAACTACAAGCCCGAAGAATAA-3′, into the GFP-expressing pG-SUPER vector (Kojima et al., 2004). SEPT2 siRNA, 5′-GGAGAACATCGTGCCCGTC-3′, and siGENOME nontargeting siRNA 1 were purchased from Thermo Fisher Scientific. SEPT2-ΔCTT was constructed by PCR amplification of SEPT2 (aa 1–315) using the primers 5′-CCGCTCGAGCCACCATGTCTAAGCAACAACC-3′ (forward) and 5′-TCTGGATCCATGTCCTCATTCTCTACTTTC-3′ (reverse) and cloning into the BamHI and XhoI sites of pEGFP-N1 (Invitrogen). SEPT2-mCherry was made by swapping the full-length SEPT2 from pEYFP-N1 into pmCherry-N1. Plasmids expressing α-tubulin–GFP and EB1-dsRed were a gift from J. Nelson (Stanford University, Stanford, CA; Barth et al., 2002).

Immunofluorescence microscopy and quantifications

Cells were fixed with 3% PFA in warm PHEM buffer (60 mM Pipes-KOH, pH 6.9, 25 mM Hepes, 10 mM EDTA, and 2 mM $MgCl_2$) containing 0.1% Triton X-100. EB1 staining required fixation with methanol at −20°C

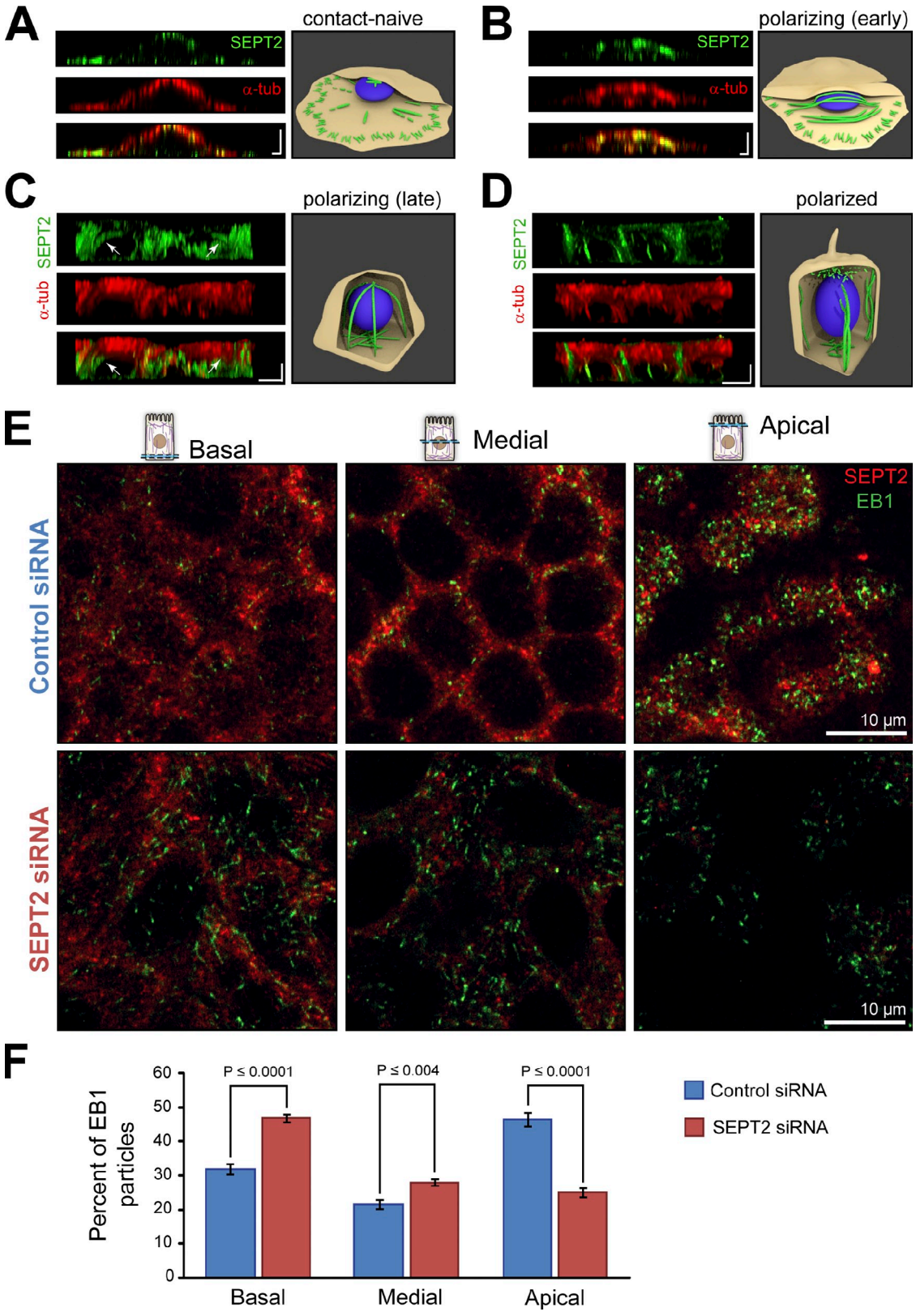

Figure 5. **Septins control the apicobasal distribution of epithelial MTs.** (A and B) Confocal xz images of contact-naive and polarizing MDCK cells stained for SEPT2 and α-tubulin. Schematics show position of SEPT2 filaments with respect to the nucleus (blue). Bars, 2.5 µm. (C and D) Side views of 3D-rendered confocal images of MDCK cells plated on Transwell filters for 12 h (late stages of polarization) and 48 h (polarized). Arrows point to SEPT2 filaments that arch from the basolateral to the apical cytoplasm. Images were γ adjusted. Bars, 5 µm. (E) Confocal microscopy slices taken from the basal, medial, and apical sections of MDCK cells (24 h on Transwell) treated with control and SEPT2 siRNAs and stained for SEPT2 and EB1. (F) Graph shows the percentage of EB1 comets distributed in the apical, medial, and basal cytoplasm of control (n = 16) and SEPT2-depleted (n = 18) MDCK cells. α-tub, α-tubulin. Error bars represent SEM.

for 5 min. Primary antibodies to EB1 (1A11/4; Santa Cruz Biotechnology, Inc.), paxillin (349; BD), SEPT2 (N5N; gift from M. Kinoshita, Nagoya University, Nagoya, Japan), SEPT6 (S6CU; gift from M. Kinoshita), SEPT7 (Immuno-Biological Laboratories, Inc.), GFP (Invitrogen), α-tubulin (DM1A; Sigma-Aldrich), and secondary donkey DyLight 488–, 549–, 594–, or 649–conjugated F(ab')$_2$ to mouse or rabbit IgG (Jackson ImmunoResearch Laboratories, Inc.) were diluted in PBS with 2% BSA. Staining with antibodies of the same species was performed with an antibody-labeling kit (Zenon; Invitrogen). Coverslips were mounted with FluorSave (EMD) or Vectashield (Vector Laboratories) and imaged on a confocal laser-scanning microscope (FluoView 1000; Olympus) using a Plan Apochromat 60×/1.42 NA objective. 0.2-µm-thick serial optical sections were acquired at 0.12-µm steps and then exported into the SlideBook 5.0 software (Intelligent Imaging Innovations) for image processing and quantification. MT and septin filament masks were created by fluorescence intensity segmentation, and the angle tool was used to measure MT angles from the major axis (Fig. 1 C) and the radius from the centroid of the cell (Fig. 2 C). Using SlideBook's macro function, we wrote a script that automatically masked MTs with fivefold intensity of the dimmest peripheral MTs and measured Manders coefficients (Fig. 1 D) and the percentage of total MT intensity (Fig. 2 B). In Fig. 5, EB1 particles were quantified in single optical sections taken at 0.6 µm from the top (apical) and bottom (basal) of each cell and halfway in between (medial). 2D projections of z stacks were performed with SlideBook's maximal projection module. 3D rendering of the z stack was performed with the Volocity software (PerkinElmer), and images were γ adjusted (Fig. 5). All datasets were statistically analyzed using an unpaired *t* test. P-values represent 95% confidence limits.

Time-lapse imaging and analysis

Spinning-disk confocal microscopy was performed at 37°C with an inverted microscope (IX-71; Olympus) equipped with a scan head (CSU10; Yokogawa), a camera (ImagEM; Hamamatsu Photonics), a 100× 1.4 NA objective, a stage-top incubator (LiveCell; Pathology Devices) and objective heater, and the MetaMorph software (Molecular Devices). In FRAP experiments, GFP was photobleached with a 435-nm pulsed nitrogen laser (MicroPoint; Photonic Instruments) controlled by the Galvo module (MicroPoint). Wide-field time-lapse imaging was performed at 37°C with a microscope (IX-81; Olympus) equipped with a motorized stage (ProScanII; Prior), a camera (Orca-R^2; Hamamatsu Photonics), a Plan Apochromat 60×/1.40 NA objective, a custom built stage-top chamber with a temperature controller (Air-Therm ATX; World Precision Instruments), and the SlideBook 5 software. SlideBook was used to make photobleach corrections, kymographs, and time-composite channels and to enhance image quality with a Difference of Gaussians algorithm and No Neighbors deconvolution. We imaged fluctuations in lateral MT movements by subtracting MT fluorescence intensities at a 15-s interval. The difference was registered and quantified as a new fluorescence channel. Tracking of EB1 dynamics was performed at 2–3-s intervals within a 5-µm-wide zone (periphery) along the free edge of the cell and an area (cell interior) delimitated by the border of this region and the nucleus. Unidirectional displacements of a distance >0.2 µm and velocity >0.05 µm/s were scored as growth or shrinkage. Displacements with distances and speeds below these values were scored as attenuation (Panda et al., 1995). Displacements of >0.7 µm were empirically determined as catastrophes. In Fig. 4 D, EB1 comets that did not move for >6 s while intersecting with the lattice of another MT were scored as pausing. Angles of incidence between EB1 trajectories and MT lattices (Fig. 4 F) were measured with SlideBook's angle tool.

Online supplemental material

Fig. S1 shows SEPT6 and SEPT7 localization in control and SEPT2 knockdown cells and the proliferation of SEPT2 filaments upon treatment with paclitaxel. Fig. S2 shows that MT side to side movements increase in SEPT2 knockdown cells and demonstrates the loss of perinuclear bundles after expression of SEPT2-ΔCTT-GFP. Fig. S3 shows localization of endogenous EB1 with respect to SEPT2-YFP in subconfluent and confluent monolayers of MDCKs. The videos show EB1 moving on perinuclear SEPT2 filaments (Video 1); MT ends growing along SEPT2 (Video 2); MT ends docking and turning onto SEPT2-coated MTs (Video 3); EB1 tracking on peripheral SEPT2 fibers (Video 4); and 3D images of SEPT2 and MT localization in contact-naive (Video 5), polarizing (Videos 6 and 7), and polarized (Video 8) MDCK cells. Online supplemental material is available at http://www.jcb.org/cgi/content/full/jcb.201102076/DC1.

We thank Andrea Stout (Cell and Developmental Biology Microscope Core, University of Pennsylvania, Philadelphia, PA) and undergraduates Tina Mathew and Peter Saira for technical help. We are grateful to Drs. James Nelson and Makoto Kinoshita for reagents.

This study was, in part, supported by the National Institutes of Health grant NS48090, a Drexel University Commonwealth Universal Research Enhancement award from the Commonwealth of Pennsylvania Tobacco Settlement Fund, and the Antelo Devereux Award for Young Faculty (to E.T. Spiliotis).

Submitted: 15 February 2011
Accepted: 22 June 2011

References

Akhmanova, A., and M.O. Steinmetz. 2008. Tracking the ends: a dynamic protein network controls the fate of microtubule tips. *Nat. Rev. Mol. Cell Biol.* 9:309–322. doi:10.1038/nrm2369

Amir, S., and N.J. Mabjeesh. 2007. SEPT9_V1 protein expression is associated with human cancer cell resistance to microtubule-disrupting agents. *Cancer Biol. Ther.* 6:1926–1931. doi:10.4161/cbt.6.12.4971

Applewhite, D.A., K.D. Grode, D. Keller, A.D. Zadeh, K.C. Slep, and S.L. Rogers. 2010. The spectraplakin Short stop is an actin-microtubule cross-linker that contributes to organization of the microtubule network. *Mol. Biol. Cell*. 21:1714–1724. (published erratum appears in *Mol. Biol. Cell.* 2010. 21:2097) doi:10.1091/mbc.E10-01-0011

Bacallao, R., C. Antony, C. Dotti, E. Karsenti, E.H. Stelzer, and K. Simons. 1989. The subcellular organization of Madin-Darby canine kidney cells during the formation of a polarized epithelium. *J. Cell Biol.* 109:2817–2832. doi:10.1083/jcb.109.6.2817

Barth, A.I., K.A. Siemers, and W.J. Nelson. 2002. Dissecting interactions between EB1, microtubules and APC in cortical clusters at the plasma membrane. *J. Cell Sci.* 115:1583–1590.

Bertin, A., M.A. McMurray, P. Grob, S.S. Park, G. Garcia III, I. Patanwala, H.L. Ng, T. Alber, J. Thorner, and E. Nogales. 2008. *Saccharomyces cerevisiae* septins: supramolecular organization of heterooligomers and the mechanism of filament assembly. *Proc. Natl. Acad. Sci. USA*. 105:8274–8279. doi:10.1073/pnas.0803330105

Bratman, S.V., and F. Chang. 2008. Mechanisms for maintaining microtubule bundles. *Trends Cell Biol.* 18:580–586. doi:10.1016/j.tcb.2008.09.004

Bré, M.H., T.E. Kreis, and E. Karsenti. 1987. Control of microtubule nucleation and stability in Madin-Darby canine kidney cells: the occurrence of noncentrosomal, stable detyrosinated microtubules. *J. Cell Biol.* 105:1283–1296. doi:10.1083/jcb.105.3.1283

Bré, M.H., R. Pepperkok, A.M. Hill, N. Levilliers, W. Ansorge, E.H. Stelzer, and E. Karsenti. 1990. Regulation of microtubule dynamics and nucleation during polarization in MDCK II cells. *J. Cell Biol.* 111:3013–3021. doi:10.1083/jcb.111.6.3013

Browning, H., J. Hayles, J. Mata, L. Aveline, P. Nurse, and J.R. McIntosh. 2000. Tea2p is a kinesin-like protein required to generate polarized growth in fission yeast. *J. Cell Biol.* 151:15–28. doi:10.1083/jcb.151.1.15

Buendia, B., M.H. Bré, G. Griffiths, and E. Karsenti. 1990. Cytoskeletal control of centrioles movement during the establishment of polarity in Madin-Darby canine kidney cells. *J. Cell Biol.* 110:1123–1135. doi:10.1083/jcb.110.4.1123

Carvalho, P., M.L. Gupta Jr., M.A. Hoyt, and D. Pellman. 2004. Cell cycle control of kinesin-mediated transport of Bik1 (CLIP-170) regulates microtubule stability and dynein activation. *Dev. Cell*. 6:815–829. doi:10.1016/j.devcel.2004.05.001

Caudron, F., and Y. Barral. 2009. Septins and the lateral compartmentalization of eukaryotic membranes. *Dev. Cell*. 16:493–506. doi:10.1016/j.devcel.2009.04.003

Chausovsky, A., A.D. Bershadsky, and G.G. Borisy. 2000. Cadherin-mediated regulation of microtubule dynamics. *Nat. Cell Biol.* 2:797–804. doi:10.1038/35041037

Cohen, D., P.J. Brennwald, E. Rodriguez-Boulan, and A. Müsch. 2004. Mammalian PAR-1 determines epithelial lumen polarity by organizing the microtubule cytoskeleton. *J. Cell Biol.* 164:717–727. doi:10.1083/jcb.200308104

Cox, D.N., B. Lu, T.Q. Sun, L.T. Williams, and Y.N. Jan. 2001. *Drosophila* par-1 is required for oocyte differentiation and microtubule organization. *Curr. Biol.* 11:75–87. doi:10.1016/S0960-9822(01)00027-6

Dixit, R., and R. Cyr. 2004. Encounters between dynamic cortical microtubules promote ordering of the cortical array through angle-dependent modifications of microtubule behavior. *Plant Cell*. 16:3274–3284. doi:10.1105/tpc.104.026930

Doerflinger, H., R. Benton, J.M. Shulman, and D. St Johnston. 2003. The role of PAR-1 in regulating the polarised microtubule cytoskeleton in the

Drosophila follicular epithelium. *Development*. 130:3965–3975. doi:10.1242/dev.00616

Downing, K.H. 2000. Structural basis for the interaction of tubulin with proteins and drugs that affect microtubule dynamics. *Annu. Rev. Cell Dev. Biol.* 16:89–111. doi:10.1146/annurev.cellbio.16.1.89

Hotta, A., T. Kawakatsu, T. Nakatani, T. Sato, C. Matsui, T. Sukezane, T. Akagi, T. Hamaji, I. Grigoriev, A. Akhmanova, et al. 2010. Laminin-based cell adhesion anchors microtubule plus ends to the epithelial cell basal cortex through LL5α/β. *J. Cell Biol.* 189:901–917. doi:10.1083/jcb.200910095

Jaulin, F., and G. Kreitzer. 2010. KIF17 stabilizes microtubules and contributes to epithelial morphogenesis by acting at MT plus ends with EB1 and APC. *J. Cell Biol.* 190:443–460. doi:10.1083/jcb.201006044

Joberty, G., R.R. Perlungher, P.J. Sheffield, M. Kinoshita, M. Noda, T. Haystead, and I.G. Macara. 2001. Borg proteins control septin organization and are negatively regulated by Cdc42. *Nat. Cell Biol.* 3:861–866. doi:10.1038/ncb1001-861

Joo, E., M.C. Surka, and W.S. Trimble. 2007. Mammalian SEPT2 is required for scaffolding nonmuscle myosin II and its kinases. *Dev. Cell*. 13:677–690. doi:10.1016/j.devcel.2007.09.001

Kaverina, I., K. Rottner, and J.V. Small. 1998. Targeting, capture, and stabilization of microtubules at early focal adhesions. *J. Cell Biol.* 142:181–190. doi:10.1083/jcb.142.1.181

Kinoshita, M., S. Kumar, A. Mizoguchi, C. Ide, A. Kinoshita, T. Haraguchi, Y. Hiraoka, and M. Noda. 1997. Nedd5, a mammalian septin, is a novel cytoskeletal component interacting with actin-based structures. *Genes Dev.* 11:1535–1547. doi:10.1101/gad.11.12.1535

Kinoshita, M., C.M. Field, M.L. Coughlin, A.F. Straight, and T.J. Mitchison. 2002. Self- and actin-templated assembly of Mammalian septins. *Dev. Cell*. 3:791–802. doi:10.1016/S1534-5807(02)00366-0

Kodama, A., I. Karakesisoglou, E. Wong, A. Vaezi, and E. Fuchs. 2003. ACF7: an essential integrator of microtubule dynamics. *Cell*. 115:343–354. doi:10.1016/S0092-8674(03)00813-4

Kojima, S., D. Vignjevic, and G.G. Borisy. 2004. Improved silencing vector co-expressing GFP and small hairpin RNA. *Biotechniques*. 36:74–79.

Kremer, B.E., T. Haystead, and I.G. Macara. 2005. Mammalian septins regulate microtubule stability through interaction with the microtubule-binding protein MAP4. *Mol. Biol. Cell*. 16:4648–4659. doi:10.1091/mbc.E05-03-0267

Krylyshkina, O., K.I. Anderson, I. Kaverina, I. Upmann, D.J. Manstein, J.V. Small, and D.K. Toomre. 2003. Nanometer targeting of microtubules to focal adhesions. *J. Cell Biol.* 161:853–859. doi:10.1083/jcb.200301102

Kulic, I.M., A.E. Brown, H. Kim, C. Kural, B. Blehm, P.R. Selvin, P.C. Nelson, and V.I. Gelfand. 2008. The role of microtubule movement in bidirectional organelle transport. *Proc. Natl. Acad. Sci. USA*. 105:10011–10016. doi:10.1073/pnas.0800031105

Kusch, J., A. Meyer, M.P. Snyder, and Y. Barral. 2002. Microtubule capture by the cleavage apparatus is required for proper spindle positioning in yeast. *Genes Dev.* 16:1627–1639. doi:10.1101/gad.222602

Maffini, S., A.R. Maia, A.L. Manning, Z. Maliga, A.L. Pereira, M. Junqueira, A. Shevchenko, A. Hyman, J.R. Yates III, N. Galjart, et al. 2009. Motor-independent targeting of CLASPs to kinetochores by CENP-E promotes microtubule turnover and poleward flux. *Curr. Biol.* 19:1566–1572. doi:10.1016/j.cub.2009.07.059

McMurray, M.A., and J. Thorner. 2009. Septins: molecular partitioning and the generation of cellular asymmetry. *Cell Div.* 4:18. doi:10.1186/1747-1028-4-18

Mellman, I., and W.J. Nelson. 2008. Coordinated protein sorting, targeting and distribution in polarized cells. *Nat. Rev. Mol. Cell Biol.* 9:833–845. doi:10.1038/nrm2525

Mimori-Kiyosue, Y., I. Grigoriev, G. Lansbergen, H. Sasaki, C. Matsui, F. Severin, N. Galjart, F. Grosveld, I. Vorobjev, S. Tsukita, and A. Akhmanova. 2005. CLASP1 and CLASP2 bind to EB1 and regulate microtubule plus-end dynamics at the cell cortex. *J. Cell Biol.* 168:141–153. doi:10.1083/jcb.200405094

Mogensen, M.M., J.B. Tucker, J.B. Mackie, A.R. Prescott, and I.S. Näthke. 2002. The adenomatous polyposis coli protein unambiguously localizes to microtubule plus ends and is involved in establishing parallel arrays of microtubule bundles in highly polarized epithelial cells. *J. Cell Biol.* 157:1041–1048. doi:10.1083/jcb.200203001

Mostov, K., T. Su, and M. ter Beest. 2003. Polarized epithelial membrane traffic: conservation and plasticity. *Nat. Cell Biol.* 5:287–293. doi:10.1038/ncb0403-287

Müsch, A. 2004. Microtubule organization and function in epithelial cells. *Traffic*. 5:1–9. doi:10.1111/j.1600-0854.2003.00149.x

Nagata, K., A. Kawajiri, S. Matsui, M. Takagishi, T. Shiromizu, N. Saitoh, I. Izawa, T. Kiyono, T.J. Itoh, H. Hotani, and M. Inagaki. 2003. Filament formation of MSF-A, a mammalian septin, in human mammary epithelial cells depends on interactions with microtubules. *J. Biol. Chem.* 278:18538–18543. doi:10.1074/jbc.M205246200

Oh, Y., and E. Bi. 2011. Septin structure and function in yeast and beyond. *Trends Cell Biol.* 21:141–148. doi:10.1016/j.tcb.2010.11.006

Panda, D., B.L. Goode, S.C. Feinstein, and L. Wilson. 1995. Kinetic stabilization of microtubule dynamics at steady state by tau and microtubule-binding domains of tau. *Biochemistry*. 34:11117–11127. doi:10.1021/bi00035a017

Pepperkok, R., M.H. Bré, J. Davoust, and T.E. Kreis. 1990. Microtubules are stabilized in confluent epithelial cells but not in fibroblasts. *J. Cell Biol.* 111:3003–3012. doi:10.1083/jcb.111.6.3003

Reilein, A., and W.J. Nelson. 2005. APC is a component of an organizing template for cortical microtubule networks. *Nat. Cell Biol.* 7:463–473. doi:10.1038/ncb1248

Rodriguez-Boulan, E., and W.J. Nelson. 1989. Morphogenesis of the polarized epithelial cell phenotype. *Science*. 245:718–725. doi:10.1126/science.2672330

Rodriguez-Boulan, E., G. Kreitzer, and A. Müsch. 2005. Organization of vesicular trafficking in epithelia. *Nat. Rev. Mol. Cell Biol.* 6:233–247. doi:10.1038/nrm1593

Sammak, P.J., and G.G. Borisy. 1988. Direct observation of microtubule dynamics in living cells. *Nature*. 332:724–726. doi:10.1038/332724a0

Spiliotis, E.T. 2010. Regulation of microtubule organization and functions by septin GTPases. *Cytoskeleton (Hoboken)*. 67:339–345.

Spiliotis, E.T., M. Kinoshita, and W.J. Nelson. 2005. A mitotic septin scaffold required for Mammalian chromosome congression and segregation. *Science*. 307:1781–1785. doi:10.1126/science.1106823

Spiliotis, E.T., S.J. Hunt, Q. Hu, M. Kinoshita, and W.J. Nelson. 2008. Epithelial polarity requires septin coupling of vesicle transport to polyglutamylated microtubules. *J. Cell Biol.* 180:295–303. doi:10.1083/jcb.200710039

Su, L.K., M. Burrell, D.E. Hill, J. Gyuris, R. Brent, R. Wiltshire, J. Trent, B. Vogelstein, and K.W. Kinzler. 1995. APC binds to the novel protein EB1. *Cancer Res.* 55:2972–2977.

Waterman-Storer, C.M., W.C. Salmon, and E.D. Salmon. 2000. Feedback interactions between cell-cell adherens junctions and cytoskeletal dynamics in newt lung epithelial cells. *Mol. Biol. Cell*. 11:2471–2483.

Wittmann, T., and C.M. Waterman-Storer. 2005. Spatial regulation of CLASP affinity for microtubules by Rac1 and GSK3β in migrating epithelial cells. *J. Cell Biol.* 169:929–939. doi:10.1083/jcb.200412114

Zhu, M., F. Wang, F. Yan, P.Y. Yao, J. Du, X. Gao, X. Wang, Q. Wu, T. Ward, J. Li, et al. 2008. Septin 7 interacts with centromere-associated protein E and is required for its kinetochore localization. *J. Biol. Chem.* 283:18916–18925. doi:10.1074/jbc.M710591200

Zumbrunn, J., K. Kinoshita, A.A. Hyman, and I.S. Näthke. 2001. Binding of the adenomatous polyposis coli protein to microtubules increases microtubule stability and is regulated by GSK3 beta phosphorylation. *Curr. Biol.* 11:44–49. doi:10.1016/S0960-9822(01)00002-1